Multiscale Modeling of a CAMILA Hall Thruster Discharge

IEPC-2017-311

Presented at the 35th International Electric Propulsion Conference
Georgia Institute of Technology – Atlanta, Georgia – USA
October 8–12, 2017

Matteo Laterza* and Igal Kronhaus†
Faculty of Aerospace Engineering, Technion, Haifa, 3200003, Israel

A multiscale model was developed for the channel of a CoAxial Magnetically Insulated Long Anode (CAMILA) Hall effect thruster. The computational domain was subdivided into a region where a hybrid solver is used and a region where a fully kinetic particle in cell solver is used. An interface was developed to transmit particles and field data between the two different solvers. The multiscale simulation results were compared to a fully kinetic simulation as well as experimental results. The results show the usefulness of this type of approach for modeling complex variants of Hall thrusters.

Nomenclature

B_r = radial component of the magnetic field.

B_z = axial component of the magnetic field.

e = electron unit charge.

E_e = electron internal energy.

I_a = total anode current.

I_e = total electron current.

I_i = total ion current.

I_w = total current to the walls.

k_B = Boltzmann constant.

$\mu_{e\perp}$ = electron mobility across field lines.

n_e = electron number density.

n_i = ion number density.

Q_{cond} = conductive energy transfer.

Q_{conv} = convective energy transfer.

S_h = ohmic losses.

S_i = inelastic losses.

*Postdoctoral Fellow, Aerospace Plasma Laboratory, mlaterza@technion.ac.il
†Head, Aerospace Plasma Laboratory, kronhaus@technion.ac.il

T_e = electron temperature.

u_e = electron drift velocity.

u_i = ion drift velocity.

W_p = work of electron pressure.

$\vec{V}$ = particle velocity array.

$\vec{X}$ = particle position array.

ϕ = plasma potential.

ϕ_L = Laplace component of plasma potential.

ϕ_P = Poisson component of plasma potential.

ϕ^* = thermalized potential.

λ = coordinate for quasi 1D temperature solution.

ρ = charge density.

I. Introduction

When a thruster passes from a laboratory model to a commercial one, lifetime evaluation becomes of major importance. Experimental lifetime tests cost a great amount of time and resources. To tackle this problem, a variety of numerical solvers for modeling the HALL thruster discharge have been developed.[1–4] Since lifetime in Hall thrusters is closely linked to erosion, numerical models need to be fast enough to adapt to changing boundary conditions and be able to simulate hundreds of hours of real operation in a self consistent way. One common solver is the so-called hybrid code.[2,4,5]

In hybrid fluid-PIC codes, the heavy species are modelled using the traditional Particle-In-Cell (PIC) method, while electrons are modeled as a fluid. This allows to overcome the major performance limitations of fully kinetic PIC codes, in which the mesh size and time step of the simulation are limited by the Debye length and electron plasma frequency, respectively.

The cost for this increase in performance, however, is that stronger assumptions must be made in the properties of the plasma inside the thruster. One example is the hybrid model used in HPHall2,[5,6] where electrons cooled down by ceramic walls have a much higher thermal conductivity along magnetic field lines than across them. This means that the electron temperature can be considered constant along field lines, which in turn implies that the thermalized potential[7] , defined in Eq. (1), can be also considered constant along the lines.

$$\phi^* = \phi - \frac{k_B T_e}{e} \ln(n_e) \tag{1}$$

Here ϕ^* is the thermalized potential, ϕ is the plasma potential, k_B is the Boltzmann constant, T_e is the electron temperature, e is the electron unit charge and n_e is the electron number density. Using the above approach the 2D problem of computing plasma potential in the rz domain can be described by quasi one dimensional equations across field lines. This assumption works well for traditional Hall thrusters. However, for non conventional designs such as the CAMILA (Co-Axial Magnetically Insulated Long Anode) Hall thruster the current approach fails to model the discharge correctly.

The CAMILA Hall thruster is an innovative low power thruster $\approx 150W$ with excellent performance for its class.[8] The working principle of the CAMILA concept has been described in depth in previous publications.[9] The CAMILA Hall thruster channel in Fig. 1 divides the acceleration channel into an anode region, where longitudinal anodes run along the channel center line, and an acceleration region, surrounded by short traditional ceramic walls. The combination of long wall-anodes and the chosen magnetic field structure generates a radial electric field that retard ions from the walls in the plasma generation region, resulting in higher propellant utilization efficiency than classical Hall thrusters.

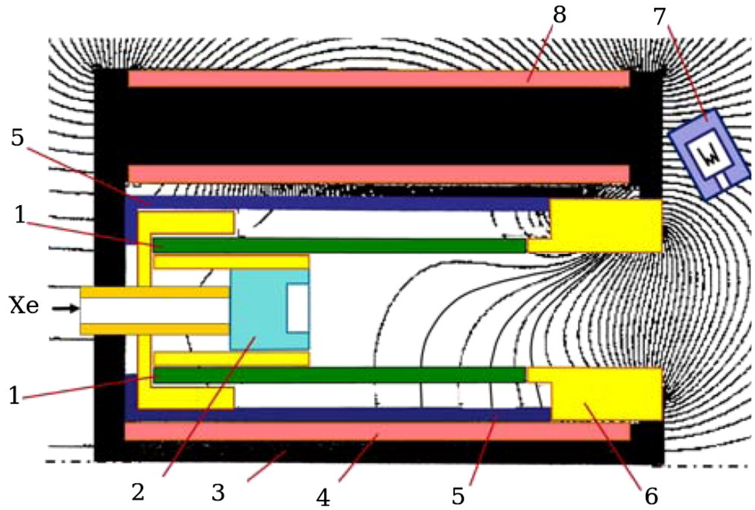

Figure 1. CAMILA Hall thruster: 1 anodes; 2 gas distributor; 3 magnetic circuit; 4,8 main coils; 5 magnetic shields; 6 ceramic channel; 7 cathode. Taken from Ref.[9]

Numerous problems with the hybrid model are immediately evident in the anode region of the CAMILA thruster . First of all, magnetic field lines end at the anodes, where electrons are not cooled but absorbed. Second, and most importantly, field lines run in this region mostly along the z direction and crossing different region of the plasma; several magnetic field lines also intercept the same anode, which is by definition at a constant potential. This does not allow for a semi one dimensional solution to the problem. Lastly, the presence of cusps in the magnetic field would require branching in the solution of the problem.

In this paper we present a multiscale hybrid model for plasma inside the channel of a CAMILA thruster, which is adequately fast and physically accurate. The model is compared with an existing PIC solution and experimental data.

II. Numerical Methods

A. Architecture

As stated in the introduction, for the CAMILA Hall thruster the assumptions of hybrid models are not satisfied in the entirety of the channel but only in the region of the ceramic channel walls. The model is, however, reliable in the acceleration region of the channel itself. This is also the region where the plasma is the densest, which creates the heaviest computational burden on PIC codes. In the anode region the plasma is rarefied enough that a fully kinetic PIC code, which is able to capture the complex dynamics of this area, is practical. We therefore propose a method to simultaneously solve both regions using an interface between the two numerical solvers.

The general structure of the code is based on XOOPIC, a general purpose PIC plasma code developed at Berkeley.[10] This object-oriented code supports well modifications and the additions of new models, and modified versions of it have been successfully used at the Aerospace Plasma Lab (APL), Technion. The code is termed XOOPIC-APL.

Another advantage of XOOPIC is that it allows for multiple simulation regions, working on different processor cores and communicating through MPI (Message Passing Interface) protocols. The code was modified to allow for different solvers in different regions and an interface had to be developed. The rest of this chapter is divided in three sections. The first will briefly describe the properties of XOOPIC-APLl electrostatic solver, used in the anode region, will the second and the third sections will describe the main modifications part of this work: the hybrid solver and the region interface, respectively.

B. Electrostatic solver

XOOPIC-APL provides different options for particle pushers and field solvers. In our case we used a simple electrostatic solver, using the leapfrog and Boris methods for particle push. The magnetic field is considered constant, and it is loaded at the beginning of the simulation. The initial magnetic field is computed externally through the open source software *femm*.[11]

The electric potential was computed using the native DADI (Dynamic Alternating Direction Implicit) solver.[12] The anode boundaries are represented by equipotential surfaces, while the dielectric walls are modeled as dielectric surfaces with surface charge deposition. The bottom wall of the chamber, where the gas distributor is placed, is a floating conductor; its potential is computed through the native current source boundary[13] by imposing a net current of zero.

The interface boundary is detailed in section D

C. Hybrid solver

The hybrid solver is based on the model developed by Fife and Martinez-Sanchez for HPHall[5] and the modifications developed by Parra and Ahedo for HPHall2.[6]

As outlined in the introduction, the model is based on dividing the computational domain in "cells" built around magnetic field lines. In each cell the electron temperature and thermalized potential are considered constant.

Figure 2 shows the PIC grid and the superimposed magnetic field lines.

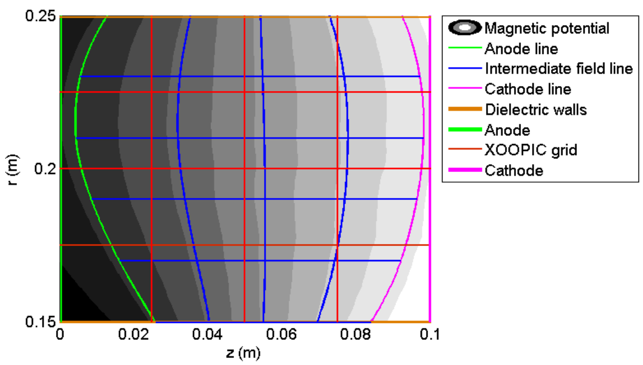

Figure 2. Computational domain of the hybrid solver.

It would be theoretically possible to use the grid constructed for the hybrid solver as the only grid in the hybrid section of the solver. Such an approach however has a number of drawbacks. First of all, the XOOPIC code was build around a rectilinear grid geometry, and changing it with a curvilinear grid requires significant changes to the code. It would also make the communication between regions more complicated. Keeping separate grids allows for more freedom in choosing the optimal mesh size for the two different models. The price for this choice is that number density values have to be interpolated from the PIC grid to the magnetic grid, and the potential has to be interpolated back. Another problem lies with the two areas between the anode and cathode lines and the edges of the PIC grid. Our approach is to designate the area at ground potentia out of boundaries. On the anode side it was decided to linearly interpolate the potential from the SRB boundary, which is a copy of the PIC boundary, to the first magnetic field line. This should not constitute a great source of inaccuracy, since in the considered area the potential is mostly uniform.

Figure 3 represents the structure of a single hybrid grid cell.

Similar to Fife[5] the cell is defined through the $\lambda\chi$ coordinate system. Here λ is defined by:

$$\frac{\partial \lambda}{\partial z} = rB_r, \frac{\partial \lambda}{\partial r} = -rB_z \tag{2}$$

This formulation guarantees that λ is constant along a field line. The χ coordinate is instead just an integration variable along field lines.

The energy balance in each cell can be written as:

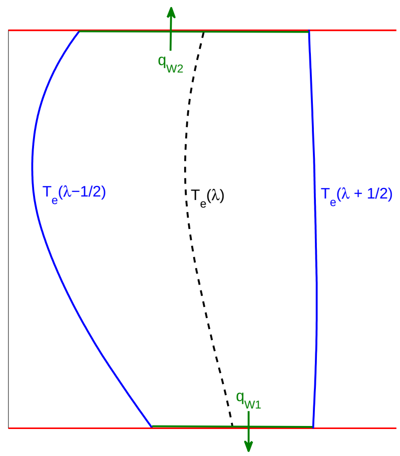

Figure 3. Representation of a hybrid grid cell for the computation of electron temperature, at coordinate λ.

$$\frac{\partial E_e}{\partial t} + Q_{conv} + Q_{cond} + W_p = S_h - S_i \tag{3}$$

where E_e is the electron internal energy, Q_{conv} and Q_{cond} are the convective and conductive components of the energy transfer through the cell boundaries, W_p is the work of electron pressure, S_h represents the ohmic heating and S_i represents the inelastic losses for excitation and ionization.

Equation 3 can be reduced to:

$$\frac{\partial T_e}{\partial t} = f\left(T_e, \frac{\partial T_e}{\partial \lambda}, n_i, u_i\right) \tag{4}$$

using the following assumptions: first quasineutrality is maintained; secondly ion properties are constant within a timestep; and third T_e is considered uniform within a single cell.

Equation 4 can be discretized and solved using the Forward Time Centered Space (FTCS) method.

In addition we impose current continuity in the cell.

$$I_a = I_e + I_i + I_w \tag{5}$$

where I_e is the total electron current, I_i is the total ion current and I_w is the current to the walls.

Using Eqs. 1 and 2, we can write the electron current as:

$$I_e = \iint_S k_B n_e u_e dS = \iint_S k_B n_e \mu_{e\perp} \left(-rB\frac{\partial \phi^*}{\partial \lambda} - rB\frac{k_B}{e}(\ln(n_e) - 1)\frac{\partial T_e}{\partial \lambda}\right) dS \tag{6}$$

where $\mu_{e\perp}$ is the electron mobility across magnetic field lines.

If the anode current is given, we can invert Eq. 6 and combine it with Eq. 5 to obtain $\partial\phi^*/\partial\lambda$ as a function of T_e, ion current, and ion number density, given quasineutrality. This function can now numerically be integrated to obtain the thermalized potential drop across the domain, from which the plasma potential drop can be obtained through Eq. 1. Since the input variable is the potential drop and not the anode current, the process is iterated using the Newton method to find the actual anode current for a given potential drop. The densities of neutrals and ions are obtained from the macroparticle data, since both these species are modeled as particles in the hybrid code. The integration of Eq. 4 requires for the electron temperature to be known at the boundaries. Electron temperature at the cathode boundary is prescribed, but the temperature at the anode boundary must be an output of the hybrid solver. For the temperature boundary both a constant value condition and a constant first derivative condition were tried. The last input is the potential drop in the acceleration region. This is readily obtained by fixing the cathode potential and importing the boundary potential from the electrostatic solver.

D. Interface

The interface between different computational regions is handled by APL-XOOPIC creating two linked artificial boundaries in the neighboring regions, called Spatial Region Boundaries (SRBs). These SRBs, however, were designed to interface computational domains using the same model. In this case, the two regions require and provide different kind of information.

Table 1. representation of the exchange of data through the SRB.

Anode region - electrostatic solver	
Variables used	
$\vec{X}_e, \vec{V}_e, \vec{X}_i, \vec{V}_i, \vec{X}_n, \vec{V}_n, \phi, \phi(Anode)$	
Variables sent to SRB	Variables received from SRB
ϕ(SRB), $\vec{X}_i, \vec{V}_i, \vec{X}_n, \vec{V}_n$	$\vec{X}_e, \vec{V}_e$
Acceleration region - hybrid solver	
Variables sent to SRB	Variables received from SRB
$\vec{X}_i, \vec{V}_i, \vec{X}_n, \vec{V}_n, T_e(SRB), I_e(SRB)$	$\vec{X}_i, \vec{V}_i, \vec{X}_n, \vec{V}_n, \phi(SRB)$
Variables used	
$\vec{X}_i, \vec{V}_i, \vec{X}_n, \vec{V}_n, \phi(SRB), \phi(Cathode)T_e$	

Table 1 lists the variables in use in each computational domain, and the variables exchanged between the domains. We note that some of the exchanges are one directional. This directionality of exchange is explained by the fact that the PIC is a full kinetic description of the plasma while the hybrid code is an approximation. Specifically the hybrid part solver ignores the electron macro-particle data generated by the PIC. The hybrid solver only considers the net current of electrons, so electrons crossing back the boundary on the electrostatic region are not used by the SRB. On the other hand Electrons needed by the electrostatic solver are generated by the SRB starting from fluid data provided by the hybrid region, i.e. electron current and temperature.

The second directional exchange involves the electric potential. While the electrostatic solver does not need a boundary potential to be defined on all of the boundaries, the hybrid solver needs a defined potential drop. The potential is thus self-consistently computed in the electrostatic region, and the boundary potential is passed to the hybrid one.

SRBs act in APL-XOOPIC as any other boundary, and are called in three phases of the computational cycle: when pushed particles intersect boundaries, when boundary conditions for advancing fields need to be imposed, and when new particles are emitted before the following step.

In the first case, SRBs act like free space, collecting the particles and removing them from the simulation. Ions and neutrals are then passed to the linked boundary to be stored for the emission phase.

During the field advance phase, the SRBs on the two sides act differently. A word must be spent here on how the DADI solver works in the electrostatic case. The solver uses the superposition properties of the Poisson equation to decrease the computational burden. The plasma potential ϕ is computed as the sum of a Poisson component ϕ_P and of as many Laplace components ϕ_L as there are boundaries. The Poisson component ϕ_P is obtained by solving the Poisson equation $\nabla\phi_P = \rho$ with space and surface charge contributions while grounding the boundaries. For any boundary i, the Laplace solution is solved by setting $\phi_i = 1$ and solving for the Laplace equation $\nabla\phi_L = 0$. In this way at every cycle the the Laplace solution needs not to be computed again, even in the case of time-dependent boundaries, and plasma potential is obtained as:

$$\phi = \phi_P + \sum_i \phi_{Li}\phi_i \tag{7}$$

On the PIC side, the SRB acts again as free space, imposing dielectric condition on the Laplace solution. It affects the Poisson solution only indirectly by emitting electrons. The SRB on the hybrid side, instead, copies the boundary potential from the PIC SRB. The hybrid field solver module then uses the potential value of the point closest to the anode magnetic field line as potential drop for its solution.

During the emission phase, both SRBs emit the ion and neutral acroparticles in the position and at the velocity passed by their linked boundary. On the PIC side the boundary has to emit the proper distribution of electron macroparticles. The quasineutrality assumption of the hybrid model is extended to the boundary, and the number density of the electrons to be emitted is matched to the one of the ions in the half cells facing the SRB. The axial electron current traversing the boundary, as well as the electron temperature, is provided by the hybrid module through the linked SRB. This information is also used to also generate the velocity distribution of the emitted electron macroparticles.

III. Simulation Results

A. Domain subdivision

The test case used for verifying the multiscale model is a fully kinetic simulation of the CAMILA Hall thruster channel performed by Kronhaus.[14] It was possible to directly load the particle data with the code native functions in the new model. Figure 4 shows the computational domain. The two anodes are set at a potential of 300V, while the cathode boundary is grounded. Two different SRB locations along the thruster channel were examined.

Since the hybrid formulation does not allow for cusps, the position labeled as SRB- 2 is such that the loop in the magnetic field at the top of the channel is outside the hybrid solver region. This boundary is also placed near the edge of the potential fall in the magnetized area, as shown in Fig. 5. The drawback of this choice is that a large portion of the high density plasma, shown in gray scale in the figure, is still in the PIC region, increasing computational costs.

In the case of the SRB - 1, instead, all the high density plasma is contained in the hybrid region, which is preferable. In this case the first magnetic field line touches the anode. As stated before, the hybrid model only allows for dielectric walls. In this case, however, only the first line touches the anode, so the walls are properly dealt with as dielectric in the solver. The main drawback of this choice of SRB is that in a large portion of the domain the potential is simply interpolated and not directly computed.

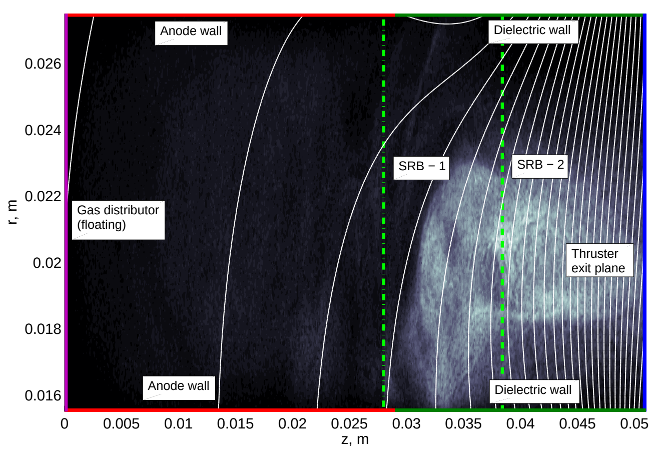

Figure 4. Representation of the computational domain and its boundaries. Gray scale represents plasma density, while the magnetic field lines are in white.

Figure 5 shows the resulting potential profile for the two choices of SRB, compared with the PIC solution in the entire domain. Solid lines represent the PIC solution in different domains, while dashed and dash-dot lines represent hybrid solutions.

B. Laplace correction

The first thing to notice in Fig. 5 is that the PIC solutions with domain subdivision diverge from the PIC solution of the whole domain, leading to an erroneous starting potential for the hybrid solver. This happens because with the decomposition the Laplace contribution is not considered. This can be solved by computing

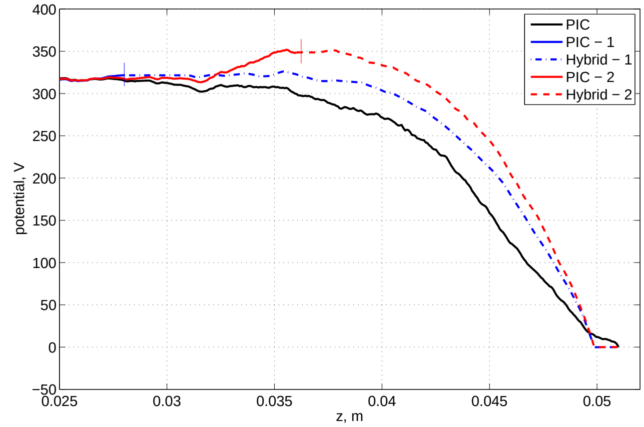

Figure 5. Plasma potential profiles at the channel centerline for the PIC case and the two different placements of SRB.

the Laplace contribution on the whole domain before the simulation starts and the use the superposition in the PIC section at following steps. Figure 6 shows the comparison of the hybrid results with and without the correction. The Laplace correction influences case 2 much more than it does case 1, since the vacuum potential between the anodes is almost unaffected by the cathode. Both cases are anyway now closer to the PIC values.

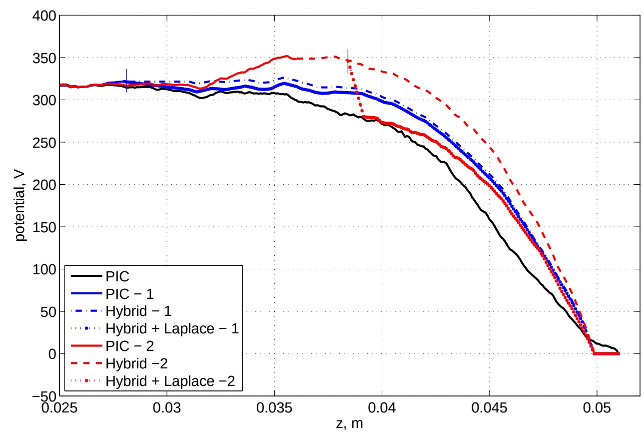

Figure 6. Plasma potential profiles at the channel centerline for the PIC case and the two different placements of SRB, compared with the hybrid solution with Laplace corrected initial conditions.

C. Temperature and grid dependence

We now examine more in detail the lesser discrepancies that still remain between the PIC and hybrid predicted potentials. We analize next sources of possible errors in the multiscale approach. The first aspect is the sampling of ion macroparticles. The grid size required for stability of the PIC solver corresponds in this case to a mesh size of $0.08mm$. The resulting number density distribution is very noisy, leading to much higher gradients than physically expected. Since the hybrid solver is not bounded by the stability restrictions of the PIC code, a coarser grid was chosen with a mesh size of $0.3mm$. The second aspect is electron temperature. The hybrid model seems to underestimate the electron temperature along the channel. The literature seems to address wall loss models as a major factor in temperature errors.[15,16] It is also shown that ion sampling can lead to wall loss overestimations. To test this hypothesis several tests were conducted with the wall losses set to zero. Figure 7 shows electron temperature estimations of the PIC model, the coarse-grid hybrid model and the hybrid model without wall losses. It is evident how wall losses play a major role in electron temperature errors.

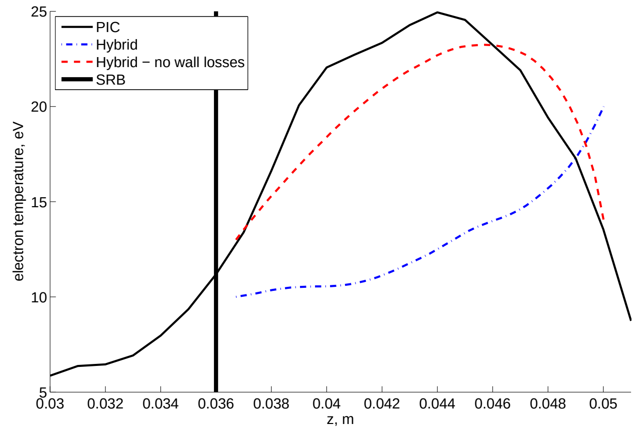

Figure 7. Eletron temperature profiles along the channel in the PIC case compared with a coarse grid version of the hybrid model, with and without wall losses.

None the less if we look at the potential profile along the channel in Fig. 8, we see that both models provide a good prediction of the plasma potential.

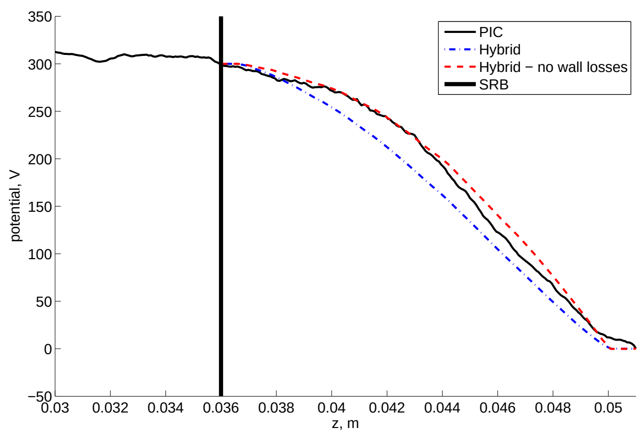

Figure 8. Plasma potential profiles at the channel centerline for the PIC case and a coarse grid version of the hybrid model, with and without wall losses.

While the temperature correction does improve the prediction on the axial profile, its contribution can be better seen looking at potential contours on the computational domain, as shown in Fig. 9.

D. Experimental value comparison

Another test was performed by comparing the hybrid solution to experimental data instead of the PIC data. These data were obtained using Langmuir and emissive probes.[9] As shown in Fig. 11 the plasma does not reach the cathode potential at the boundary. Therefore for the purpose of this comparison we matched the hybrid boundary to the measured potential. It has to be noted that the particle data used to obtain the ion density and current for the hybrid model are still the ones of the PIC solution, which will add some error.

Both SRB locations were tested. Wall losses were not set artificially to zero for this comparison, but regularly computed. The boundary condition for the electron temperature model was not in this case the

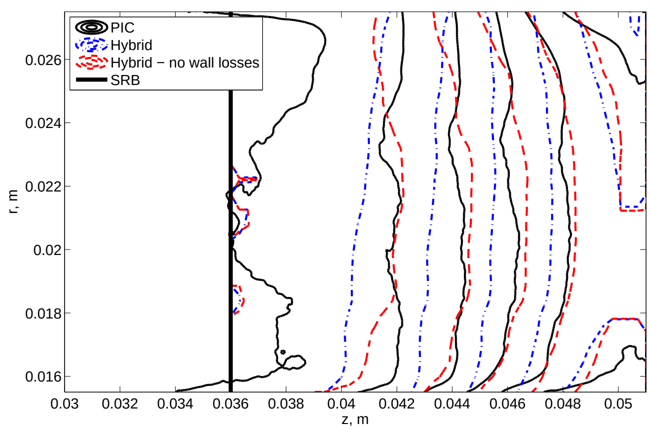

Figure 9. Plasma potential contours in zr coordinates for the PIC case and a coarse grid version of the hybrid model, with and without wall losses.

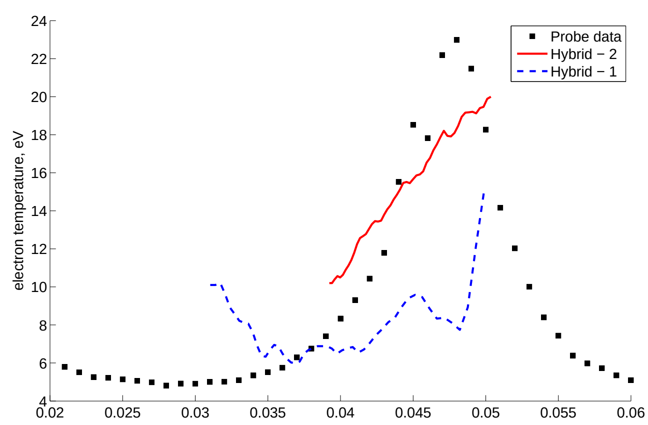

Figure 10. Electron temperature profiles along the channel for the experimental data and the two different placements of SRB.

cathod temperature but the temperature measured at the boundary. Figure 10 shows that the higher electron temperature at the boundary leads to temperatures closer to the experimental values throughout the domain, especially in the SRB-2 case.

We conclude that the temperatures are close enough to the measured value to give a satisfactory prediction of plasma potential values. Figure 11 shows the potential profile obtained from experimental measurements compared with the results of both configurations. Both results show good agreement. We note that the multiscale model seems to agree better with experimental results that it does with the fully kinetic PIC simulation. It is particularly interesting that the SRB-1 configuration manages to follow the potential profile, since using this configuration can lead to a much better performance of the code in term of computational costs.

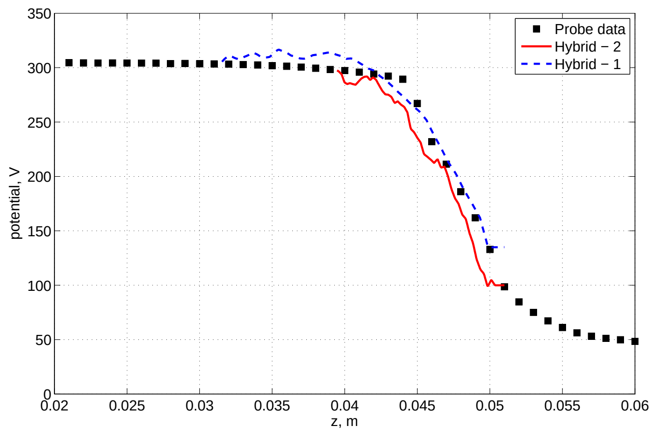

Figure 11. Plasma potential profiles at the channel centerline for the experimental data and the two different placements of SRB.

IV. Conclusions

A multiscale simulation of the CAMILA Hall thruster discharge is being developed at the Aerospace Plasma Laboratory, Technion. The simulation supports different numerical solvers using spatial decomposition. In the region of high density plasma the code utilizes a hybrid solver while in the near anode region, where the plasma is less dense and the boundary conditions more complex, a fully kinetic solver is utilized. After proper selection of the position of the interference between the solvers, it was shown that the multiscale simulation results agree well with a proven fully kinetic simulation and experimental data. The current stage of the simulation supports only particle transfer between the model regions. In the near future a fully dynamic simulation including ionization and recombination processes will be developed. It is also planned to asses the speed increase factor of the multiscale simulation compared to a fully kinetic simulation.

Aknowledgements

The work was sponsored by the Israeli Ministry of Defense (Maf'at) in the project "Multiscale Hall Thruster Simulation".

References

[1] John T Yim, Michael Keidar, and Iain D Boyd. A hydrodynamic-based erosion model for hall thrusters. In *29th International Electric Propulsion Conference, IEPC-2005-013, Princeton, NJ*, 2005.

[2] Shannon Y Cheng and Manuel Martinez-Sanchez. Hybrid particle-in-cell erosion modeling of two hall thrusters. *Journal of Propulsion and Power*, 24(5):987–998, 2008.

[3] Richard R Hofer, Ioannis G Mikellides, Ira Katz, and Dan M Goebel. Bpt-4000 hall thruster discharge chamber erosion model comparison with qualification life test data. In *30th International Electric Propulsion Conference*, pages 17–20, 2007.

[4] Emmanuelle Sommier, Michelle K Allis, Nicolas Gascon, and Mark A Cappelli. Wall erosion in 2d hall thruster simulations.

AIAA Paper, 4656, 2006.

[5] John Michael Fife. *Hybrid-PIC modeling and electrostatic probe survey of Hall thrusters*. PhD thesis, Massachusetts Institute of Technology, 1998.

[6] FI Parra, E Ahedo, JM Fife, and M Martinez-Sanchez. A two-dimensional hybrid model of the hall thruster discharge. *Journal of Applied Physics*, 100(2):023304, 2006.

[7] AI Morozov and VV Savelyev. Fundamentals of stationary plasma thruster theory. In *Reviews of plasma physics*, pages 203–391. Springer, 2000.

[8] A Kapulkin, V Balabanov, M Rubanovich, E Behar, L Rabinovich, and A Warshavsky. Camila hall thruster: New results. In *International Electric Propulsion Conference*, pages 2011–046, 2011.

[9] Igal Kronhaus, Alexander Kapulkin, Vladimir Balabanov, Maksim Rubanovich, Moshe Guelman, and Benveniste Natan. Discharge characterization of the coaxial magnetoisolated longitudinal anode hall thruster. *Journal of Propulsion and Power*, 29(4):938–949, 2013.

[10] John P Verboncoeur, A Bruce Langdon, and NT Gladd. An object-oriented electromagnetic pic code. *Computer Physics Communications*, 87(1-2):199–211, 1995.

[11] David Meeker. Finite element method magnetics. *FEMM*, 4:32, 2010.

[12] PJ Mardahl and JP Verboncoeur. Charge conservation in electromagnetic pic codes; spectral comparison of boris/dadi and langdon-marder methods. *Computer physics communications*, 106(3):219–229, 1997.

[13] Vahid Vahedi and G DiPeso. Simultaneous potential and circuit solution for two-dimensional bounded plasma simulation codes. *Journal of Computational Physics*, 131(1):149–163, 1997.

[14] Igal Kronhaus, Alexander Kapulkin, Moshe Guelman, and Benveniste Natan. Investigation of two discharge configurations in the camila hall thruster by the particle-in-cell method. *Plasma Sources Science and Technology*, 21(3):035005, 2012.

[15] FI Parra, E Ahedo, M Martinez-Sanchex, and Michael Fife. Improvement of the plasma-wall model on a fluid-pic code of a hall thruster. In *4th International Spacecraft Propulsion Conference*, volume 555, 2004.

[16] Richard R Hofer, Ioannis G Mikellides, Ira Katz, and Dan M Goebel. Wall sheath and electron mobility modeling in hybrid-pic hall thruster simulations. *AIAA Paper*, 5267:2007, 2007.